Journal of Environmental Monitoring

Cite this: *J. Environ. Monit.*, 2011, **13**, 3420

www.rsc.org/jem

PAPER

Cycling of rare earth elements in the atmosphere in central Tokyo

Yoshinari Suzuki, Shimpei Hikida and Naoki Furuta*

Received 22nd July 2011, Accepted 26th September 2011
DOI: 10.1039/c1em10590f

Concentrations of 14 rare earth elements (REEs) in six size classes of airborne particulate matter (APM) (<0.43, 0.43–0.65, 0.65–1.1, 1.1–2.1, 2.1–11, and >11 μm) and in two different phases (suspended particulate and dissolved) in rainwater were determined by inductively coupled plasma mass spectrometry (ICP-MS). Positive Eu and Tb anomalies were observed in size-classified APM. These anomalies may be due to large emissions of Eu and Tb to the atmosphere resulting from the recent change in Japan from the use of cathode-ray tubes to plasma displays in television sets (Eu and Tb) and from the widespread use of magneto-optical disks (Tb). The light REEs were enriched in fine APM particles (diameter < 1.1 μm). Because compositions of La/Ce/Sm in fine APM (diameter < 1.1 μm) were similar to those in automobile catalyst, the light REE enrichment was attributed to automobile emissions. In contrast, the REE distribution pattern in the suspended particulate phase in rainwater was similar to that in coarse APM (diameter > 2.1 μm), and a positive Tb anomaly was observed, suggesting that coarse particles easily become trapped in rain droplets. A negative Eu anomaly was observed in the dissolved phase in rainwater, but not in APM or in the suspended particulate phase in rainwater. Unlike other REEs, Eu can exist as both bivalent and trivalent ions in nature, and Eu-selective dissolution from or adsorption onto the trapped particles of Eu might account for the negative anomaly. These results show that atmospheric REE cycling is affected by the physico-chemical properties of APM.

Introduction

All of the rare earth elements (REEs) have similar physico-chemical properties, and they have become technologically, environmentally, and economically important materials because of their versatility and specificity. Nowadays, REEs are used in various industrial and medical materials, including in ceramics for superconductors, catalysts for automobiles (La and Ce), lasers (Nd), permanent magnets (Nd, Sm, Gd, Dy, and Pr), fluorescent imaging by color televisions (Y, Eu, and Tb), fluorescent lamps (Y, La, Ce, Eu, Gd, and Tb), contrast media for magnetic resonance imaging (Gd), and fiber optic telecommunication cables (Er). As a result, large amounts of REEs are consumed.[1,2] Because about 97% of REEs are produced in China,[3] all other countries must import them from China. The expansion of demand for REEs due to industrial development has led to the development of technologies for REE recycling from used products. Because of the widespread use of REEs, it is probable that large amounts of REEs are emitted into the atmosphere.

Airborne particulate matter (APM) has become a serious air pollution problem. Many studies have investigated organic, metallic, and ionic contaminants in size-classified APM. Unlike organic compounds, heavy metals and trace elements are not biochemically decomposed and thus persist for a long time in the environment. Elements of anthropogenic origin that have been identified in APM include toxic elements such as As, Cd, Cr, Pb,

Faculty of Science and Engineering, Department of Applied Chemistry, Chuo University, 1-13-27 Kasuga, Bunkyo-ku, Tokyo, 112-8551, Japan. E-mail: nfuruta@chem.chuo-u.ac.jp

Environmental impact

In this paper, we determined concentrations of 14 rare earth elements (REEs) in six size classes and two different phases of rainwater, and then we clarified REE cycling in atmospheric environment from the physico-chemical aspect. Some REEs were enriched in APM and suspended particulate phase of rainwater because of human activities. Coarse APMs were easily trapped in rain droplet. Eu anomalies were observed only in the dissolved phase of rainwater, because of Eu-selective dissolution from or adsorption onto the trapped particles. As far as known, these are the most precise data of REE concentrations in six size classes and two different phases of rainwater at the same time.

and Hg,[4–13] and platinum-group elements such as Pt, Pd, and Rh, which are emitted from automobiles.[13–18] However, despite the widespread use of REEs, few studies have investigated them in APM collected in mountain[1] and urban areas.[19–22] Therefore, it is important to consider atmospheric REEs in evaluating the effects of atmospheric pollution on human health.

The toxic characteristics of APM depend on its aerodynamic diameter. For example, coarse particles can be filtered out by nose hairs and throat mucus whereas finer particles may be delivered into the bronchial tubes and deposited deep inside the lung.[23] Epidemiological research conducted in six cities in the United States found a significant correlation between mortality rates and the concentration of fine particles with a diameter of <2.5 μm in atomosphere.[24, 25] Because APM has a long residence time in the atmosphere, it can be transported over long distances by atmospheric circulation, and both the vertical distribution pattern and residence time of APM depend on its aerodynamic diameter.[26] APM is not only dry deposited onto land surfaces, but also can be taken up by rainwater and wet deposited. The scavenging efficiency of APM by raindrops depends on factors such as the APM diameter and rainfall intensity. Simulations have shown that coarse APM (>2 μm) is easily scavenged by wet precipitation.[27] In our previous paper,[22] we determined REE concentrations in 10 APM samples but we did not discuss about REEs in size-classified APM precisely. Therefore, it is important to determine REE concentrations in rainwater as well as in size-classified APM to assess REE cycling in the atmosphere.

To our knowledge, only four studies have reported high-precision data of REE concentrations in rainwater.[28–31] Among these, only Sholkovitz *et al.*[28] compared REE concentrations between rainwater (in both suspended particulate and dissolved phases) and aerosols. However, they investigated only 10 of 14 REEs and did not collect size-classified samples of aerosols. In this study, we collected size-classified APM samples and samples of both suspended particulate and dissolved phases in rainwater. We then determined REE concentrations by ICP-MS. Finally, on the basis of our results, we evaluated REE cycling in the atmosphere.

Experimental

Sampling

APM and rainwater were collected on the rooftop (approximately 45 m above the ground) of a building on the Chuo University campus, in Bunkyo-ku, Tokyo, Japan. APM was sampled for 25 days out of every month from April 2010 to January 2011. Six size classes of APM with aerodynamic diameters of <0.43, 0.43–0.65, 0.65–1.1, 1.1–2.1, 2.1–11, and >11 μm were collected on cellulose acetate membrane filters by using an Andersen low-volume air sampler (Model AN-200; Tokyo Dylec Co., Tokyo, Japan) with a sampling flow rate of 28.3 L min^{-1}. Cellulose acetate membrane filters (0.8 μm, i.d. 80 mm, Advantech Co. Ltd., Tokyo, Japan) were used because this material is less contaminated with REEs than the quartz glass fiber filters generally used for APM collection.[22]

Eleven rainwater samples were collected, on 12 and 27 April, 7 and 23 May, 18 June, 29 July, 10 August, 23 and 26 September, and 24 and 28 October. A polyethylene bottle with a polyethylene funnel (i.d. 30 cm) was cleaned with 5 mol L^{-1} nitric acid and ultrapure water. This bottle was set out at the beginning of the rainfall at the same sampling point of APM. After 500 mL of rainwater had been collected, the bottles were immediately picked up. In four of the 11 rainwater samples, the weight of the suspended particulate phase was sufficient for the analysis of REE concentrations in the suspended particles.

Sample preparation of size-classified APM

Following a previously reported method,[4] 6 mL of 70% HNO_3, 3 mL of 30% HF, and 1 mL of 50% H_2O_2 were added to each sample, and then the samples were digested in a microwave digestion system (MLS 1200, Milestone, Sorisole, Italy). After microwave digestion, HF was evaporated by heating the solution on a hot plate at 230 °C. After the solution was reduced to one transparent droplet (*ca.* 0.5 mL), it was diluted with Milli-Q water to 50 g. An internal standard (Re) was added during the dilution.

Rainwater sample preparation

Rainwater samples for measurement of the suspended particulate and dissolved phases were filtered through a 0.45 μm nitrocellulose filter (HAWP04700, Nihon Millipore K.K., Tokyo, Japan). The suspended particulates on the filter were digested with mixed acids by the same method as was used for the APM samples. Then, 1.0 g of nitric acid was added to 99 g of the filtered rainwater sample, and the sample was heated on a hot plate at 230 °C in a Teflon® beaker covered with a Teflon® watch glass. After heating for 2.5 h, the sample weight was readjusted to 99 g. The pH of both solutions (containing the digested suspended particulates and the dissolved phase) was adjusted to 3.0 with ammonium hydroxide (20%, TAMAPURE-AA-100, impurity <100 ng L^{-1}, Tama Chemicals Co. Ltd., Kanagawa, Japan) and acetic acid (30%, TAMAPURE-AA-100, impurity <100 ng L^{-1}, Tama Chemicals Co. Ltd., Kanagawa, Japan).

ICP-MS measurements

To analyze the APM samples, an HP 4500 ICP-MS system (Yokogawa Analytical Systems, Tokyo, Japan) with a conventional glass concentric nebulizer was used. ICP-MS was conducted under the following conditions: radiation frequency power, 1400 W; plasma gas flow rate, 15.0 L min^{-1}; auxiliary gas flow rate, 1.00 L min^{-1}; and carrier gas flow rate, 1.00 L min^{-1}. To determine REE concentrations, spectroscopic interference by oxide and hydroxide species from Ba and light REEs must be eliminated. Numerical correction of the total ion count was carried out as previously described to eliminate this interference and obtain accurate analytical results for NIST 1648.[22]

In contrast to APM, REE concentrations in rainwater (both suspended particulate and dissolved phases) are quite low. Therefore, we used an on-line preconcentration column and a hyphenated ICP-MS method with an autosampler (ASX500, Cetac, Omaha, NE, USA) and an integrated sample introduction system (ISIS, Yokogawa Analytical Systems, Japan) for the determination. This system was installed on a clean bench (class-100) equipped with HEPA filters. For the preconcentration column, 0.4 g of MetaSEP ME-1 resin (GL Science, Japan) was

Table 1 ISIS operating sequence for matrix separation, REE preconcentration, and elution for the determination of REE concentrations in rainwater by automated on-line column preconcentration ICP-MS

Step	Solution	Flow rate/ mL min^{-1}	Time/s
1	1.5 mol L^{-1} nitric acid	2.5	90
2	Ultrapure water	2.5	60
3	0.7 mol L^{-1} ammonium acetate buffer (pH 3.0)	2.5	60
4	Sample	2.0	300
5	0.7 mol L^{-1} ammonium acetate buffer (pH 3.0)	1.0	240
6	Ultrapure water	1.0	60
7	1.5 mol L^{-1} nitric acid containing 4 μg L^{-1} of Tl as an internal standard	0.35	180

manually packed into a Teflon® tube (1.5 mm i.d. × 50 mm long). The preconcentration steps are shown in Table 1. REEs adsorbed on the chelating resin were eluted with 0.25 mL of 1.5 mol L^{-1} HNO_3 containing an internal standard element (Tl) and the resulting solution was introduced directly to the ICP-MS (Agilent 7500ce, Agilent Technologies). Numerical correction for polyatomic interference was carried out as previously described.[22] In this procedure, more than 90% of 50 pg mL^{-1} REEs were recovered. And, detection limits and analytical results of REE concentrations in the certified reference material of river water (SLRS-4) are shown in Table 2. Detection limits of REEs are sufficiently low to quantify REE concentrations in rainwater. And our analytical results showed good agreement with reported values having better precision.[30–32]

Results and discussion

Size-classified APM

Using the ICP-MS results corrected as described in the methods, we calculated the average, standard deviation, and minimum and maximum concentrations of each REE in the APM size classes (Table 3). The number of samples in which each REE was detectable is also shown in Table 3. In almost all samples, the maximum concentrations of REEs were observed in the 1.1–2.1 μm APM size class, and the minimum concentrations in the 0.43–0.65 μm size class. In the 0.43–0.64 μm APM size class, the concentrations were sometimes below the detection limit.

To determine the emission sources of atmospheric REEs collected in Tokyo, we evaluated the distribution patterns of REEs after normalizing the analytical data relative to CI meteorite concentrations. In this paper, anomaly was quantified by the following equation:

$$\text{anomaly of } \mathrm{REE}'_m = \mathrm{REE}'_m - \frac{\mathrm{REE}'_{m-1} + \mathrm{REE}'_{m+1}}{2} \quad (1)$$

In this equation, an apostrophe indicates normalized concentration by using CI meteorite and m is the atomic number. In general, REE concentrations in APM were higher in autumn and winter (October to January) and lower in summer (July to September) (Fig. 1); a similar seasonal pattern has been reported for other metals such as Sb and Pb in the Tokyo area.[4] Positive Eu and Tb anomalies were observed in almost all aerodynamic size classes of APM. Positive anomalies of Eu were observed in the >0.43 μm size classes in 6 of 10 months, and in the <0.43 μm size class in 8 of 10 months. From a thermochemical perspective, Eu is more easily released into the environment than the other REEs, because its melting (1090 K) and boiling (1870 K) points are the lowest among REEs.[33] Positive Tb anomalies were observed more frequently than Eu anomalies: in 10 of 10 months in the >1.1 μm size classes, in 9 of 10 months in the <0.43 and 0.65–1.1 μm size classes, and in 7 of 10 months in the 0.43–0.65 μm size classes. In general, Eu and Tb anomalies were seldom observed in April and May. Positive Eu and Tb anomalies in APM may be due to the large consumption of Eu and Tb resulting from the recent change in Japan from the use of cathode-ray tubes to plasma displays in television sets. Eu and Tb are used in cathode-ray tubes and plasma displays. However, recycling procedures by the manufacturer were only 40% of emission of cathode-ray tubes.[34] It was considered that Eu and Tb were emitted into the atmosphere from the waste of cathode-ray tubes rather than from production of plasma displays. Tb is

Table 2 Detection limit and analytical results of REE concentrations (pg mL^{-1}, average ± standard deviation) in the river water certified reference material SLRS-4

	Detection limit[a]	Analytical value			
Element	This study	This study	Yeghicheyan *et al.*[32b]	Shimamura *et al.*[30]	Iwashita *et al.*[31c]
La	0.034	300 ± 23	287 ± 8	290 ± 20	281 ± 10
Ce	0.16	370 ± 10	360 ± 12	360 ± 10	354 ± 12
Pr	0.006	70.1 ± 0.1	69.3 ± 1.8	65 ± 1	68 ± 2
Nd	0.11	269 ± 2	269 ± 14	290 ± 10	261 ± 8
Sm	0.012	58.2 ± 0.4	57.4 ± 2.8	57 ± 1	56 ± 2
Eu	0.07	7.77 ± 0.01	8.0 ± 0.6	9 ± 1	7.8 ± 1
Gd	0.15	36.0 ± 0.2	34.2 ± 2.0	40 ± 1	27 ± 1
Tb	0.016	4.31 ± 0.08	4.31 ± 0.4	4.7 ± 0.1	4.3 ± 0.2
Dy	0.053	23.9 ± 0.04	24.2 ± 1.6	23 ± 1	23 ± 1.2
Ho	0.021	4.54 ± 0.10	4.7 ± 0.3	4.2 ± 0.1	4.7 ± 0.2
Er	0.055	13.8 ± 0.3	13.4 ± 0.6	11 ± 1	13.5 ± 0.6
Tm	0.019	1.75 ± 0.02	1.7 ± 0.2	1.6 ± 0.1	1.9 ± 0.2
Yb	0.062	12.4 ± 0.2	12.0 ± 0.4	11 ± 1	12.5 ± 0.6
Lu	0.023	1.80 ± 0.06	1.9 ± 0.1	ND	1.7 ± 0.2

[a] Detection limit was calculated from 3σ of blank value. [b] Compilation on data obtained by 5 different laboratories. [c] No dilution.

Table 3 APM and REE concentrations (average ± standard deviation, minimum–maximum, APM and REE concentrations are expressed in μg m^{-3} and μg g^{-1}, respectively) in size-classified APM collected in central Tokyo[a]

	Aerodynamic diameter of APM/μm					
Element	<0.43	0.43–0.65	0.65–1.1	1.1–2.1	2.1–11	>11
APM	6.24 ± 1.51 4.24–9.07 *n* = 10	3.63 ± 1.84 1.15–6.32 *n* = 10	5.21 ± 1.50 2.57–7.71 *n* = 10	2.71 ± 1.39 0.63–4.66 *n* = 10	9.56 ± 3.30 3.40–14.2 *n* = 10	3.16 ± 1.28 1.33–5.13 *n* = 10
La	7.03 ± 3.24 2.91–12.1 *n* = 10	5.53 ± 4.08 1.45–12.7 *n* = 10	4.10 ± 2.11 1.56–8.30 *n* = 10	14.2 ± 11.5 4.34–38.0 *n* = 10	11.6 ± 7.63 2.94–25.8 *n* = 10	6.64 ± 5.24 2.07–18.3 *n* = 10
Ce	15.7 ± 7.39 6.54–27.1 *n* = 10	11.2 ± 8.57 2.89–26.9 *n* = 10	6.52 ± 3.97 2.14–14.2 *n* = 10	18.3 ± 15.8 5.49–51.9 *n* = 10	17.8 ± 11.4 4.78–37.1 *n* = 10	11.9 ± 7.87 4.09–26.5 *n* = 10
Pr	1.29 ± 0.50 0.652–2.04 *n* = 10	0.783 ± 0.495 0.247–1.69 *n* = 10	0.452 ± 0.262 0.156–0.935 *n* = 10	1.31 ± 1.09 0.349–3.78 *n* = 10	1.72 ± 1.17 0.459–3.51 *n* = 10	1.09 ± 0.64 0.482–2.24 *n* = 10
Nd	4.12 ± 1.51 2.00–6.17 *n* = 10	2.94 ± 2.14 0.788–6.37 *n* = 10	1.68 ± 1.17 0.511–4.19 *n* = 10	5.64 ± 5.43 1.17–18.6 *n* = 10	6.77 ± 4.66 1.90–14.3 *n* = 10	4.86 ± 3.09 2.14–10.5 *n* = 10
Sm	0.156 ± 0.081 0.050–0.336 *n* = 10	0.060 ± 0.032 n.d.–0.123 *n* = 6	0.131 ± 0.071 n.d.–0.251 *n* = 9	0.749 ± 0.662 0.211–2.33 *n* = 10	1.21 ± 0.78 0.368–2.41 *n* = 10	0.885 ± 0.457 0.501–1.89 *n* = 10
Eu	0.073 ± 0.038 0.014–0.129 *n* = 10	0.066 ± 0.084 0.017–0.275 *n* = 10	0.056 ± 0.037 0.021–0.138 *n* = 10	0.303 ± 0.303 0.100–1.11 *n* = 10	0.472 ± 0.284 0.181–1.11 *n* = 10	0.401 ± 0.246 0.174–0.900 *n* = 10
Gd	0.163 ± 0.086 0.042–0.299 *n* = 10	0.161 ± 0.127 0.052–0.390 *n* = 10	0.140 ± 0.074 0.057–0.303 *n* = 10	0.996 ± 0.864 0.226–3.07 *n* = 10	1.44 ± 0.86 0.533–2.97 *n* = 10	1.15 ± 0.64 0.610–2.40 *n* = 10
Tb	0.045 ± 0.025 0.013–0.096 *n* = 10	0.027 ± 0.020 0.009–0.071 *n* = 10	0.039 ± 0.025 0.021–0.100 *n* = 10	0.242 ± 0.273 0.075–0.984 *n* = 10	0.356 ± 0.243 0.139–0.934 *n* = 10	0.245 ± 0.166 0.101–0.582 *n* = 10
Dy	0.173 ± 0.078 0.093–0.335 *n* = 10	0.106 ± 0.076 0.031–0.227 *n* = 10	0.154 ± 0.097 0.048–0.391 *n* = 10	0.950 ± 0.882 0.192–3.14 *n* = 10	1.21 ± 0.76 0.453–2.64 *n* = 10	1.03 ± 0.56 0.497–2.10 *n* = 10
Ho	0.032 ± 0.015 0.008–0.056 *n* = 10	0.014 ± 0.009 n.d.–0.031 *n* = 8	0.025 ± 0.014 0.007–0.057 *n* = 10	0.182 ± 0.179 0.034–0.652 *n* = 10	0.241 ± 0.140 0.095–0.521 *n* = 10	0.207 ± 0.109 0.109–0.455 *n* = 10
Er	0.116 ± 0.055 0.067–0.239 *n* = 10	0.059 ± 0.042 0.019–0.147 *n* = 10	0.083 ± 0.050 0.028–0.205 *n* = 10	0.529 ± 0.493 0.127–1.78 *n* = 10	0.716 ± 0.409 0.283–1.50 *n* = 10	0.625 ± 0.306 0.351–1.21 *n* = 10
Tm	0.014 ± 0.005 n.d.–0.024 *n* = 8	0.005 ± 0.002 n.d.–0.008 *n* = 7	0.010 ± 0.005 n.d.–0.020 *n* = 9	0.077 ± 0.079 0.014–0.290 *n* = 10	0.101 ± 0.056 0.042–0.208 *n* = 10	0.081 ± 0.030 0.046–0.144 *n* = 10
Yb	0.101 ± 0.044 0.047–0.188 *n* = 10	0.057 ± 0.042 0.022–0.150 *n* = 10	0.084 ± 0.053 0.025–0.216 *n* = 10	0.530 ± 0.475 0.106–1.74 *n* = 10	0.704 ± 0.390 0.277–1.53 *n* = 10	0.582 ± 0.237 0.343–1.02 *n* = 10
Lu	0.017 ± 0.007 n.d.–0.026 *n* = 8	0.007 ± 0.003 n.d.–0.013 *n* = 7	0.013 ± 0.009 n.d.–0.034 *n* = 9	0.082 ± 0.093 0.014–0.338 *n* = 10	0.108 ± 0.055 0.047–0.221 *n* = 10	0.081 ± 0.028 0.046–0.142 *n* = 10
∑REE	29.0 ± 12.5 12.9–47.9 *n* = 10	21.0 ± 15.5 5.67–48.2 *n* = 10	13.5 ± 7.74 4.90–29.3 *n* = 10	44.1 ± 37.4 14.5–127 *n* = 10	44.5 ± 28.6 12.7–94.7 *n* = 10	29.8 ± 19.4 11.7–67.8 *n* = 10

[a] n.d.: not detected.

also used in magneto-optical disks and such disks might be another source of Tb, in addition to Tb in television displays.

Light REEs (La to Nd) were increased in APM of the <1.1 μm size classes. The Nd/Sm concentration ratios (mean ± SD) in the APM size classes <0.43, 0.43–0.65, and 0.65–1.1 μm were 26.8 ± 15.3, 27.3 ± 11.0, and 14.2 ± 12.1, respectively, values which are 2.2–5.4 times those in the APM size classes 1.1–2.1 (6.6 ± 2.4), 2.1–11 (5.3 ± 0.5), and >11 μm (5.1 ± 1.0). Light REEs are used in catalysts in petroleum refining and in three-way catalytic converters. Thus, the La/Sm ratio is considered a good indicator of traffic-related pollution. High La/Sm values are often observed in areas with high traffic density, and La/Sm values in tailpipe soot of automobiles equipped with three-way catalytic converters range from 10 to 16 000.[35] We found La/Sm ratios (mean ± SD) of 44.0 ± 27.2 (<0.43 μm), 51.4 ± 24.2 (0.43–0.65 μm), 35.8 ± 25.1 (0.65–1.1 μm), 18.7 ± 7.9 (1.1–2.1 μm), 9.8 ± 2.2 (2.1–11 μm), and 6.5 ± 2.3 (>11 μm). La/Sm ratios in APM of the size classes <0.43 and 0.43–0.65 μm agree well with those in fluidized-bed catalytic cracking (FCC) catalysts (55.2 ± 23.3).[33] FCC is a widely utilized operation in petroleum refining and petrochemical manufacturing. On the other hand, we found La/Ce ratios of 0.45 ± 0.04 (<0.43 μm), 0.50 ± 0.03 (0.43–0.65 μm), 0.66 ± 0.10 (0.65–1.1 μm), 0.83 ± 0.16 (1.1–2.1 μm), 0.65 ± 0.05 (2.1–11 μm), and 0.53 ± 0.06 (>11 μm), lower values than in

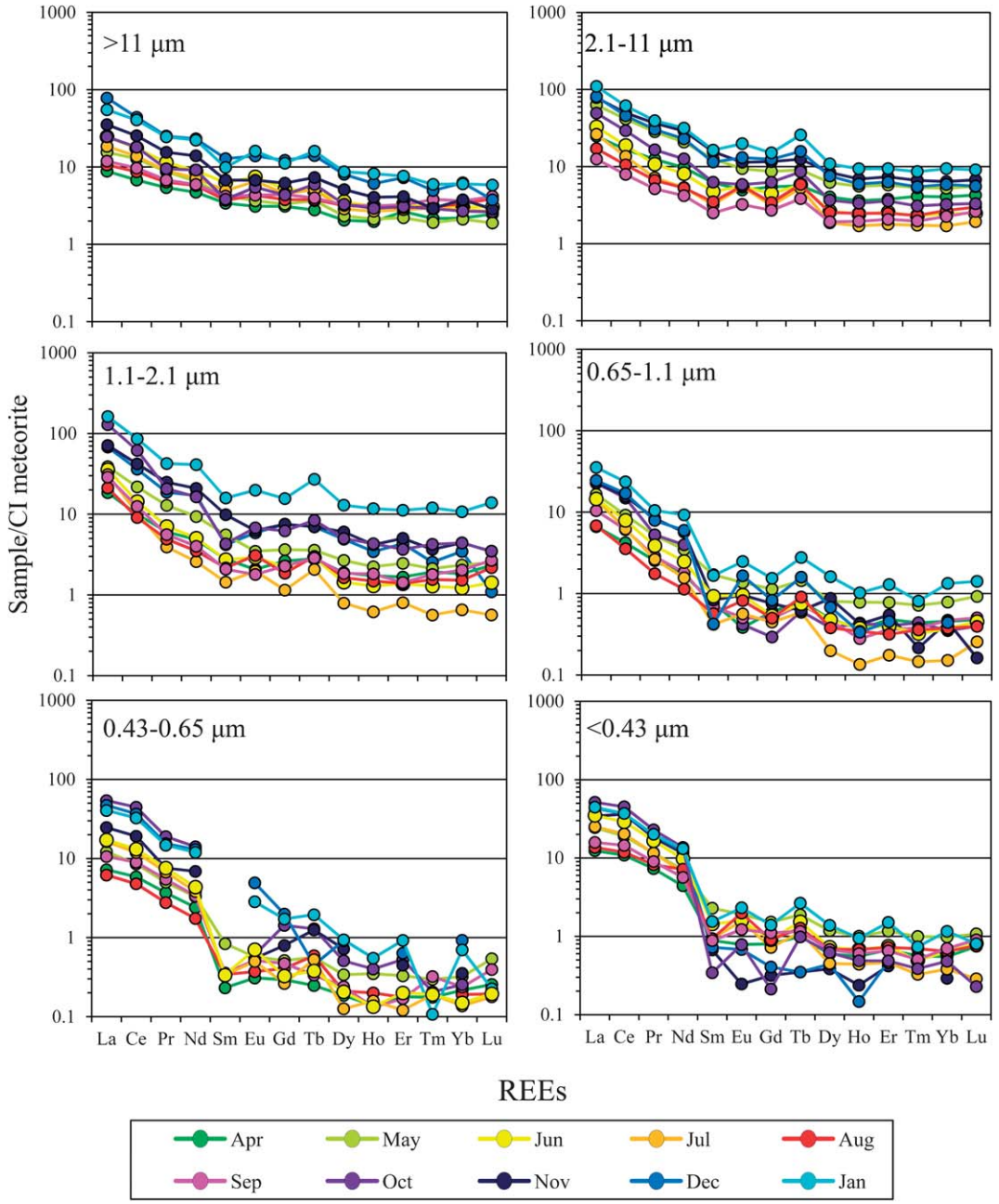

Fig. 1 CI meteorite-normalized distribution patterns of REEs in size-classified APM collected in Tokyo between April 2010 and January 2011. REE concentrations in the units of ng g^{-1} for CI meteorite were as follows: La = 234.7, Ce = 603.2, Pr = 89.1, Nd = 452.4, Sm = 147.1, Eu = 56.0, Gd = 196.6, Tb = 36.3, Dy = 242.7, Ho = 55.6, Er = 158.9, Tm = 242.2, Yb = 162.5, and Lu = 24.3.

FCC catalysts (4.3).[36] The automobile catalyst SRM 2556 is more highly enriched in Ce than in La (La/Ce = 0.70).[37] Therefore, these results suggest that APM of the <1.1 μm size classes reflects emissions from automobiles rather than from petroleum refining. The triangular diagram is shown in Fig. 2 to compare three components of La, Ce, and Sm in size-classified APM. LaCeSm compositions in APM of >2.1 μm size classes were similar to those in continental crust.[38] On the other hand, LaCeSm compositions in APM of <1.1 μm size classes were similar to those in automobile catalyst.[37] This three-component pattern was completely different from those for aerosol collected from Mexico City which was influenced by refinery.[19] These results strongly suggested that enriched La and Ce in APM of <1.1 μm size classes were originated from automobile.

Suspended particulate phase in rainwater

REE concentrations and distribution patterns in the suspended particulate phase in the rainwater samples are shown in Table 4 and Fig. 3, respectively. In general, suspended particulate phase in rainwater is considered to originate from APM, and REEs in suspended particulate phase show a distribution pattern similar to that in coarse APM particles (>1.1 μm) but not to that in fine APM particles (<1.1 μm). Positive Tb anomalies, but not positive

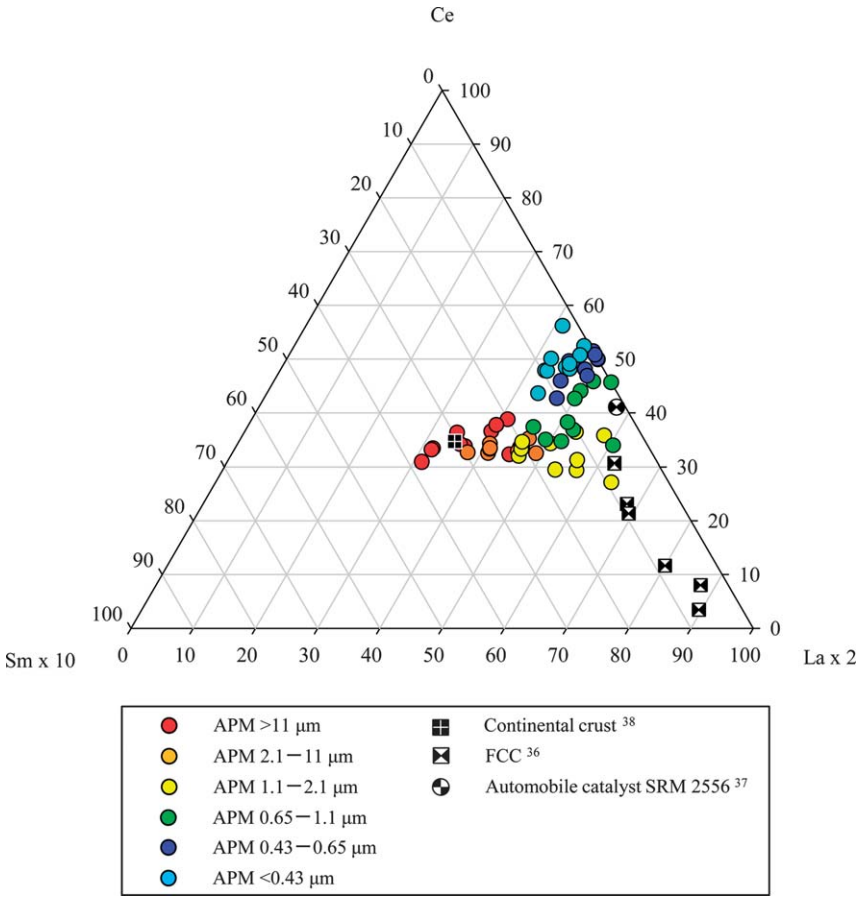

Fig. 2 Three component LaCeSm plot for size-classified APM, continental crust, and anthropogenic sources. The REE concentrations for continental crust, FCC, and automobile catalyst are from ref. 36–38, respectively.

Table 4 REE concentrations (pg mL^{-1}) in the suspended particulate phase in rainwater collected in central Tokyo in 2010

	Sampling day			
Element	23 Sep	26 Sep	24 Oct	28 Oct
La	21.0	10.3	8.15	11.1
Ce	35.2	15.5	15.9	26.4
Pr	3.05	1.56	1.53	1.82
Nd	11.6	5.87	5.98	7.18
Sm	2.43	1.15	1.15	1.25
Eu	0.877	0.269	0.391	0.413
Gd	2.53	1.16	1.22	1.95
Tb	0.594	0.184	0.237	0.345
Dy	2.32	1.02	1.06	1.26
Ho	0.462	0.215	0.195	0.227
Er	1.41	0.614	0.641	0.746
Tm	0.189	0.062	0.077	0.089
Yb	1.35	0.579	0.619	0.711
Lu	0.194	0.051	0.063	0.079

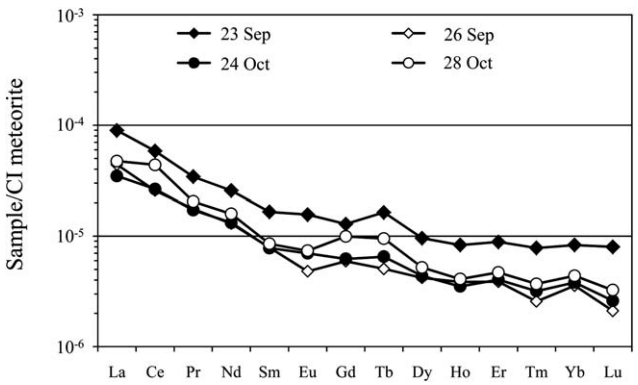

Fig. 3 CI meteorite-normalized distribution patterns of REEs in the suspended particulate phase in rainwater collected in Tokyo in September and October 2010.

Eu anomalies, were observed in these samples. The Nd/Sm concentration ratio in the suspended phase was 5.2 ± 0.4, more similar to the Nd/Sm ratio in APM of the 2.1–11 μm (5.3 ± 0.5) and >11 μm (5.1 ± 1.0) size classes compared to that in the 1.1–2.1 μm size class (6.6 ± 2.4). The increase in the ratio seen in light REEs in APM of the <1.1 μm size class was not observed in the suspended phase in rainwater. These results imply that coarse particles >2.1 μm in diameter are easily taken into raindrops; thus, the distribution pattern of REEs in the suspended particulate phase reflected that of APM particles with a diameter of >2.1 μm. Moreover, the La/Yb ratio, which represents the slope of the REE distribution, in the suspended phase (15.5 ± 1.9) was closer to the ratios in APM of the 2.1–11 μm (16.2 ± 5.5) size classes than to those in the 1.1–2.1 (30.6 ± 16.2) and >11 μm (10.5 ± 4.3) size classes. The APM concentration in the 2.1–11

μm (9.59 ± 3.30 μg m^{-3}) size class was always higher than the concentration in the other size classes as shown in Table 3, suggesting that the REE distribution pattern in the suspended particulate phase in rainwater most strongly reflected that of APM in the 2.1–11 μm class. These results agree with simulation results showing a strong increase in the scavenging coefficient for particle sizes greater than 2 μm.[27]

Dissolved phase in rainwater

REE concentrations and distribution patterns in the dissolved phase in rainwater samples are shown in Table 5 and Fig. 4, respectively. It was reported that REEs in rainwater show four distribution patterns: flat,[29,31] convex-up,[28,30,31] concave-down,[29] and light REE-enriched.[29] In this study, the average Nd/Sm (4.6 ± 0.7) and La/Yb (11.4 ± 2.5) ratios in the dissolved phase agreed well with reported values (Nd/Sm, 4.8–5.4; La/Yb, 10.1–17.6; we recalculated the ratios after converting the concentration units from mol g^{-1} to g g^{-1}) in rainwater collected at Tokyo in 1996.[29] Zhang and Liu[29] concluded that REE concentrations in rainwater collected at Tokyo normalized to shale values showed a flat distribution pattern. In our study, however, we observed negative Eu anomalies in the dissolved phase in all rainwater samples. Similarly, negative Eu anomalies have been reported in rainwater collected in Bermuda and in Delaware and Massachusetts in the United States.[28] REE anomalies of Ce and Eu are often observed because these two elements can occur in nature not only as trivalent ions, like all other REEs, but also with different valences (Ce^{4+} and Eu^{2+}). Sholkovitz *et al.*[28] suggested that geologically inherited features of minerals, namely biotite, which has a large negative Eu anomaly, and plagioclase feldspar and K-feldspar, which have large positive Eu anomalies, were transferred to precipitation. Negative Eu anomalies observed in rainwater can easily be explained because the biotite is more soluble than the feldspars. However negative Eu anomalies were not observed in any size class of APM or in the suspended particulate phase in rainwater in this study. Therefore, we do not attribute the negative Eu anomaly to a mineral origin. A more plausible explanation for the negative Eu anomaly in rainwater is

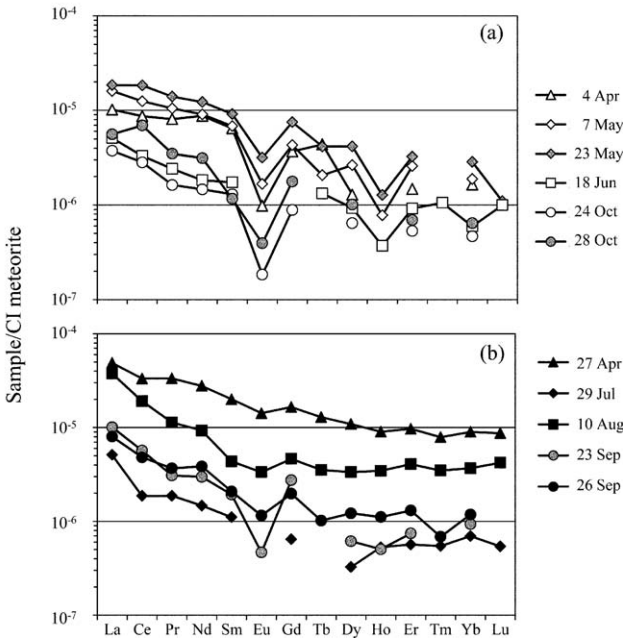

Fig. 4 CI meteorite-normalized distribution patterns of REEs in the dissolved phase in rainwater collected in Tokyo between April and October 2010. (a) Negative Ho anomaly was observed. (b) Negative Ho anomaly was not observed.

Eu-specific dissolution from or adsorption onto the trapped particles. Eu^{2+} has low solubility in water, because its hydration energy ($-\Delta H_{hydration}$), indicating its solubility in water (1458 kJ mol^{-1}), is lower than the energies of other, trivalent REEs (3278–3706 kJ mol^{-1}) and Ce^{4+} (6309 kJ mol^{-1}).[33] Moreover, Dawood *et al.*[39] attributed a negative Eu anomaly in rock collected from African coastal desert areas to adsorption of Eu onto clay minerals and coprecipitation with iron oxy-hydroxides, and we consider that Eu can easily adsorb onto suspended particulates in rainwater. These reports suggested that Eu-selective dissolution from and adsorption onto the trapped particles can explain the negative Eu anomaly in the dissolved phase in rainwater.

Table 5 REE concentrations (pg mL^{-1}) in the dissolved phase in rainwater collected in central Tokyo in 2010[a]

	Sampling day										
Element	12 Apr	27 Apr	7 May	23 May	18 Jun	29 Jul	10 Aug	23 Sep	26 Sep	24 Oct	28 Oct
La	2.39	11.5	3.76	4.34	1.20	1.20	8.84	2.36	1.88	0.878	1.31
Ce	5.24	20.1	7.54	11.1	1.99	1.13	11.5	3.43	2.91	1.70	4.18
Pr	0.721	2.98	0.936	1.25	0.215	0.167	1.01	0.275	0.328	0.145	0.310
Nd	3.96	12.6	4.11	5.55	0.829	0.665	4.20	1.35	1.74	0.663	1.41
Sm	0.951	2.94	1.01	1.35	0.256	0.163	0.640	0.283	0.306	0.191	0.171
Eu	0.055	0.797	0.094	0.177	n.d.	n.d.	0.187	0.026	0.065	0.010	0.022
Gd	0.724	3.25	0.846	1.48	n.d.	0.127	0.919	0.539	0.388	0.174	0.348
Tb	0.159	0.470	0.075	0.151	0.048	n.d.	0.128	n.d.	0.037	n.d.	n.d.
Dy	0.312	2.65	0.641	1.01	0.226	0.079	0.811	0.149	0.296	0.156	0.246
Ho	n.d.	0.503	0.043	0.071	0.021	0.029	0.192	0.028	0.062	n.d.	n.d.
Er	0.235	1.54	0.410	0.517	0.146	0.090	0.647	0.118	0.207	0.084	0.110
Tm	n.d.	0.191	n.d.	n.d.	0.025	0.013	0.084	n.d.	0.017	n.d.	n.d.
Yb	0.266	1.46	0.306	0.464	0.097	0.113	0.598	0.152	0.192	0.076	n.d.
Lu	n.d.	0.212	n.d.	0.027	0.024	0.013	0.103	n.d.	n.d.	n.d.	n.d.

[a] n.d.: not detected.

Moreover, REEs dissolved in rainwater showed two distribution patterns: with (Fig. 4a) or without (Fig. 4b) a negative Ho anomaly. No negative Ho anomaly was observed in any APM size class or in REEs in the suspended particulate phase in rainwater during the sampling period, and at this time we cannot explain the negative Ho anomaly in the dissolved phase.

Positive La and Gd anomalies were observed in rainwater collected in Sagamihara City, 35 km west of central Tokyo.[30,31] Shimamura *et al.*[30] noted that dry deposition samples and domestic wastewater showed positive Gd anomalies. They attributed the Gd anomalies to entrainment by wind of soils polluted with Gd-DTPA, a contrast agent used for magnetic resonance imaging. Previously, we observed a positive Gd anomaly in REE concentrations in water from the Kanda River and in seawater from Tokyo Bay,[40,41] which we attributed to emissions of Gd-DTPA by sewage treatment plants. However, we did not observe any positive Gd anomalies in APM and rainwater in this study. Another factor affecting REE cycling must exist that can explain the different Gd anomalies between Tokyo and Sagamihara.

REE cycling in the environment

To clarify REE cycling in the environment, we compared CI meteorite-normalized REE concentrations in size-classified APM and in the two rainwater phases with REE concentrations in the continental crust,[38] river water,[40] and seawater[41] (Fig. 5). The data about river water and seawater were referenced from our previous papers for Kanda River in Tokyo and Tokyo Bay, respectively. The light REE (La to Nd) concentration in APM was 0.091 ± 0.039 times that in the continental crust, and the intermediate to heavy REE (Nd to Lu) concentration in APM was 0.168 ± 0.064 times that in the continental crust in the <1.1 size classes, and 0.032 ± 0.016 times that in the continental crust in the >1.1 μm size classes. In water samples, REE concentrations were much lower than those in the continental crust. The REE concentration in the suspended phase in rainwater was 6.1×10^{-7} times that in the continental crust, and the concentration in the dissolved phase was 4.6×10^{-8} times that in the continental crust. In spite of the wide concentration gaps among continental crust, APM, and rainwater, the slopes of the REE distribution patterns in APM and in rainwater were similar to the pattern in the continental crust, and unlike the patterns in river water and seawater. However, there were some differences, namely, positive Eu and Tb anomalies in APM, a negative Eu anomaly in the dissolved phase in rainwater, and enrichment of light REEs (La to Nd) in APM in the <1.1 μm size classes. We therefore inferred that the atmospheric REEs originated from the continental crust but that some REEs became enriched in certain fractions as a result of human activities.

The REE distribution pattern in river water was concave-down, with a positive Gd anomaly in water from the middle reaches but not in water from the source.[40] Because the slope of the distribution pattern from La to Sm in river water was similar to that in the continental crust pattern, we attributed the enrichment in light REEs to a continental crust source. In contrast, the positive slope from Tb to Lu in the REE distribution pattern in river water was not observed in other types of samples. The stability constant for complexation of heavy REEs with organic carbon is higher than that for light REEs.[33] Heavy REE concentrations thus tend to be high in river water because they exist in complexes with organic carbon discharged into the river by human activities. The REE distribution pattern in seawater was flat with a positive Gd anomaly,[41] indicating that Gd pollution due to Gd compound emissions had been carried by the Kanda River to the sea and suggesting that light and heavy REEs might be enriched in particles settling to the seafloor.

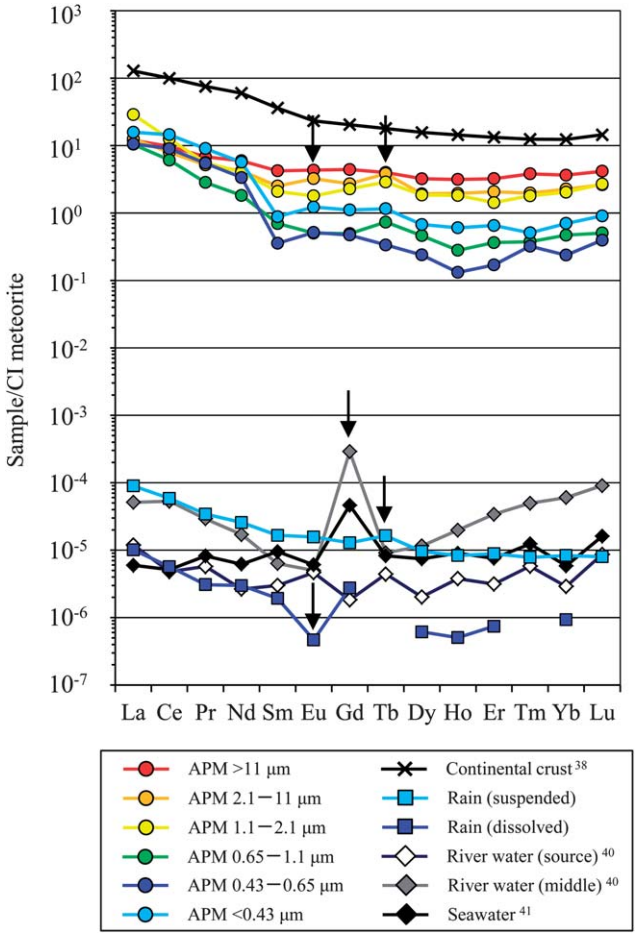

Fig. 5 CI meteorite-normalized distribution patterns of REEs in continental crust, APM, rainwater, river water (from the middle reaches or near the source), and seawater. APM collected in September and rainwater samples collected on 23 September are used here as representative examples. The REE concentrations for continental crust, river water, and seawater are from ref. 38, 40, and 41, respectively. Arrows indicate anomalies.

Conclusion

In this study, we demonstrated cycling of REEs in atmospheric environment by determination of REE concentrations in six size classes and two different phases of rainwater (suspended particulate and dissolved). As the results, positive Eu and Tb anomalies in APM and negative Eu anomaly in rainwater samples were observed. Tb anomalies in APM were observed more frequently than Eu anomalies. The positive Eu and Tb anomalies in APM may reflect the waste of Eu and Tb in cathode-ray tubes for television sets and of Tb in

magneto-optical disks. Light REEs (La–Nd) were enriched in APM of the <1.1 μm size classes. Light REEs are used in three-way catalytic converters, and we attributed their enrichment to automobile emissions. However, we did not observe this light REE enrichment in the suspended particulate phase in rainwater, where the REE distribution pattern was similar to that of APM in the 2.1–11 μm size class, indicating that coarse APM particles are more easily trapped by rainwater droplets. We observed a negative Eu anomaly in the dissolved phase in rainwater. Because Eu can exist as both bivalent and trivalent ions in nature, unlike other REEs, we inferred that Eu-selective dissolution from and adsorption onto the trapped particles could explain this negative Eu anomaly. Our findings thus indicate that atmospheric REE cycling is affected by the physico-chemical properties of APM.

Acknowledgements

We are grateful for financial support provided by the Ministry of Education, Culture, Sports, Science and Technology in Japan, through a Grant-in-Aid for Scientific Research (C) 22550081. A part of this study was supported by a joint research project entitled "Characterization of nano-scale particles in airborne particulate matter" conducted at the Institute of Science and Engineering of Chuo University.

References

1 M. Krachler, C. Mohl, H. Emons and W. Shotyk, *J. Environ. Monit.*, 2003, **5**, 111–121.
2 U.S. Geological-Survey, *USGS Fact Sheet*, 2002, 082-02.
3 U.S. Geological-Survey, *Mineral Commodity Summaries 2011*, U.S. Geological Survey, Reston, Virginia, 2011.
4 N. Furuta, A. Iijima, A. Kambe, K. Sakai and K. Sato, *J. Environ. Monit.*, 2005, **7**, 1155.
5 C. F. Wang, S. L. Jeng and F. J. Shieh, *J. Anal. At. Spectrom.*, 1997, **12**, 61–67.
6 C. F. Wang, C. J. Chin and P. C. Chiang, *Anal. Sci.*, 1998, **14**, 763–768.
7 M. Rossbach, R. Jayasekera, G. Kniewald and N. H. Thang, *Sci. Total Environ.*, 1999, **232**, 59–66.
8 A. A. A. Hameed and M. I. Khoder, *J. Environ. Monit.*, 2000, **2**, 119–121.
9 D. Bellis, C. W. McLeod and K. Satake, *J. Environ. Monit.*, 2001, **3**, 194–197.
10 D. Bellis, A. J. Cox, I. Staton, C. W. McLeod and K. Satake, *J. Environ. Monit.*, 2001, **3**, 512–514.
11 F. Goodarzi, H. Sanei and W. F. Duncan, *J. Environ. Monit.*, 2001, **3**, 515–525.
12 Y. Gao, E. D. Nelson, M. P. Field, Q. Ding, H. Li, R. M. Sherrell, C. L. Gigliotti, D. A. Van Ry, T. R. Glenn and S. J. Eisenreich, *Atmos. Environ.*, 2002, **36**, 1077–1086.
13 G. Dongarra, G. Sabatino, M. Triscari and D. Varrica, *J. Environ. Monit.*, 2003, **5**, 766.
14 B. Bocca, F. Petrucci, A. Alimonti and S. Caroli, *J. Environ. Monit.*, 2003, **5**, 563.
15 F. Petrucci, B. Bocca, A. Alimonti and S. Caroli, *J. Anal. At. Spectrom.*, 2000, **15**, 525–528.
16 M. B. Gomez, M. M. Gomez and M. A. Palacios, *J. Anal. At. Spectrom.*, 2003, **18**, 80–83.
17 L. Bencs, K. Ravindra and R. Van Grieken, *Spectrochim. Acta, Part B*, 2003, **58**, 1723–1755.
18 M. E. Kylander, S. Rauch, G. M. Morrison and K. Andam, *J. Environ. Monit.*, 2003, **5**, 91–95.
19 T. Moreno, X. Querol, A. Alastuey, J. Pey, M. C. Minguillon, N. Perez, R. M. Bernabe, S. Blanco, B. Cardenas and W. Gibbons, *Environ. Sci. Technol.*, 2008, **42**, 6502–6507.
20 C. X. Wang, W. Zhu, Z. J. Wang and R. Guicherit, *Water, Air, Soil Pollut.*, 2000, **121**, 109–118.
21 C. X. Wang, W. Zhu, A. Peng and R. Guicherit, *Environ. Int.*, 2001, **5**, 111.
22 Y. Suzuki, T. Suzuki and N. Furuta, *Anal. Sci.*, 2010, **26**, 929–935.
23 M. Lippmann and K. Ito, *Philos. Trans. R. Soc. London, Ser. A*, 2000, **358**, 2787–2797.
24 D. W. Dockery, C. A. Pope, X. P. Xu, J. D. Spengler, J. H. Ware, M. E. Fay, B. G. Ferris and F. E. Speizer, *N. Engl. J. Med.*, 1993, **329**, 1753–1759.
25 K. Ueda, H. Nitta, N. Ito and A. Mizohata, *Epidemiology*, 2009, **20**, S146.
26 T. Okuda, M. Tenmoku, J. Kato, J. Mori, T. Sato, R. Yokochi and S. Tanaka, *Water, Air, Soil Pollut.*, 2006, **174**, 3–17.
27 J. S. Henzing, D. J. L. Olivie and P. F. J. van Velthoven, *Atmos. Chem. Phys.*, 2006, **6**, 3363–3375.
28 E. R. Sholkovitz, T. M. Church and R. Arimoto, *J. Geophys. Res.*, 1993, **98**, 20587–20599.
29 J. Zhang and C.-Q. Liu, *Chem. Geol.*, 2004, **209**, 315–326.
30 T. Shimamura, M. Iwashita, S. Iijima, M. Shintani and Y. Takaku, *Atmos. Environ.*, 2007, **41**, 6999–7010.
31 M. Iwashita, A. Saito, M. Arai, Y. Furusho and T. Shimamura, *Geochem. J.*, 2011, **45**, 187–197.
32 D. Yeghicheyan, J. Carignan, M. Valladon, M. B. Le Coz, F. Le Cornec, M. Castrec-Rouelle, M. Robert, L. Aquilina, E. Aubry, C. Churlaud, A. Dia, S. Deberdt, B. Dupr, R. Freydier, G. Gruau, O. Henin, A. M. de Kersabiec, J. Mace, L. Marin, N. Morin, P. Petitjean and E. Serrat, *Geostand. Geoanal. Res.*, 2001, **25**, 465–474.
33 S. Cotton, *Lanthanide And Actinide Chemistry*, John Wiley & Sons, Ltd., West Sussex, 2006, p. 280.
34 Ministry of the Environment, http://www.env.go.jp/council/03haiki/y0311-07.html, 14th September 2011.
35 A. Mizohata, *J. Aerosol Res. Jpn.*, 1986, **1**, 274.
36 P. Kulkarni, S. Chellam and M. P. Fraser, *Atmos. Environ.*, 2006, **40**, 508–520.
37 P. J. Silva and K. A. Prather, *Environ. Sci. Technol.*, 1997, **31**, 3074–3080.
38 K. H. Wedepohl, *Geochim. Cosmochim. Acta*, 1995, **59**, 1217–1232.
39 Y. H. Dawood, H. H. A. El-Naby and A. A. Sharafeldin, *J. Geochem. Explor.*, 2004, **81**, 15–27.
40 S. Mito, M. Ohata and N. Furuta, *Bunseki Kagaku*, 2003, **52**, 575–582.
41 A. Tsuneto, Y. Suzuki, Y. Furusho and N. Furuta, *Bunseki Kagaku*, 2009, **58**, 623–631.

